Pigment Spectra and Intermolecular Interaction Potentials in Glasses and Proteins

I. Renge,* R. van Grondelle,[†] and J. P. Dekker[†]

*Institute of Physics, University of Tartu, Tartu, Estonia; and [†]Department of Biophysics and Physics of Complex Systems, Division of Physics and Astronomy, Faculty of Science, Vrije Universiteit, Amsterdam, The Netherlands

ABSTRACT   A model is proposed for chromophore optical spectra in solids over a wide range of temperatures and pressures. Inhomogeneous band shapes and their pressure dependence, as well as baric shift coefficients of spectral lines, selected by the frequency, were derived using Lennard-Jones potentials of the ground and excited states. Quadratic electron-phonon coupling constants, describing the thermal shift and broadening of zero-phonon lines, were also calculated. Experimentally, thermal shift and broadening of spectral holes were studied between 5 and 40 K for a synthetic pigment, chlorin, embedded in polymer hosts. The baric effects on holes were determined by applying hydrostatic He gas pressure up to 200 bar, at 6 K. Absorption spectra of pheophytin a, chlorophyll a, and β-carotene in polymers and plant photosystem II CP47 complex were measured between 5 (or 77) and 300 K, and subject to Voigtian deconvolution. A narrowing of inhomogeneous bandwidth with increasing temperature, predicted on the basis of hole behavior, was observed as the shrinking of Gaussian spectral component. The Lorentzian broadening was ascribed to optical dephasing up to 300 K in transitions with weak to moderate linear electron-phonon coupling strength. The thermal broadening is purely Gaussian in multiphonon transitions (S_2 band of β-carotene, Soret bands of tetrapyrrolic pigments), and the Lorentz process appears to be suppressed, indicating a lack of exponential dephasing. Density, polarity, polarizability, compressibility, and other local parameters of the pigment binding sites in biologically relevant systems can be deduced from spectroscopic data, provided that sufficient background information is available.

INTRODUCTION

Absorption and luminescence spectroscopy of biomolecules is a diverse and ever-expanding field. The first stains (carmine, hematoxylin, and eosin) were introduced to microbiology, cytology, and histology 150 years ago. Hundreds of dyes are commercially available today as markers of proteins, nucleic acids, individual cells, malignant tissue, etc. (1). The fluorescent diagnostics and photodynamic therapy of cancer (2), and the autofluorescent proteins (3) can be mentioned among the recent developments. Apart from the outstanding sensitivity and spatial selectivity of luminescence methods, the spectra themselves attract relatively little interest. The reason for the neglect of spectroscopic parameters may be the difficulties in the interpretation of spectra in the condensed phase. In particular, the absorption of photosynthetic pigment proteins is complicated by severe congestion, owing to simultaneous contributions of inhomogeneous broadening, vibronic coupling, and excitonic interactions (4).

The spectrum of a diluted impurity system at 0 K is obviously much simpler, being shaped by a convolution of inhomogeneous distribution of transition energies with vibronic side bands that accompany zero-phonon lines (ZPLs). Inhomogeneous broadening arises as a result of the spread of microscopic solvent shifts imposed by the disorder in the host matrix. Linear electron-phonon coupling (EPC) is responsible

for phonon side bands, present already at 0 K, as well as for anti-Stokes absorption at $T > 0$ K. Quadratic EPC (QEPC) manifests itself only at temperatures >0 K as the shift and broadening of ZPLs. Investigations of the solvent shifts (5,6), the linear EPC (7,8), and QEPC (9,10) have emerged as relatively independent branches of spectroscopy.

Absorption and fluorescence maxima in liquids can provide important molecular parameters, such as changes in dipole moments and polarizabilities on optical excitation (5,11,12). By contrast, numerous temperature studies concentrate on broadening rather than peak positions (9,10), since a density change obviously complicates the interpretation of shifts. The pure thermal, phonon-induced component of the shift can be separated using the thermal expansion and compressibility data, and the pressure-induced shifts, measured in conjunction with thermal studies (13,14). Both the shift and broadening are addressed from a common viewpoint in QEPC theory (9,10), and the scarcity of their simultaneous treatments is regrettable.

Spectral probing of the structure presumes a connection between the transition energies and the intermolecular distances or local densities. Further, the monitoring of local dynamics requires a model correlating the structure with the linear and QEPC parameters of spectra. Both goals can be achieved by considering intermolecular interaction potentials. In the first part of this article, an effective coordinate is introduced to characterize the packing density and the amount of free volume in the closest coordination layer surrounding the chromophore. Inhomogeneous band shape and QEPC constants will be derived from effective two-body

potentials of a guest-host system in the ground and excited states.

In the second part, broadband absorption of photosynthetic pigments and several related compounds is discussed. Voigtian deconvolution of the low-frequency portion of an absorption contour yields the Gaussian and Lorentzian components of spectra, enabling one to separate, tentatively, the homogeneous and inhomogeneous broadening in a wide temperature range up to 293 K.

With the aim of understanding the behavior of ZPLs, selected within the inhomogeneous distribution by frequency, the properties of spectral holes were investigated between 5 and 40 K for chlorin in polymer host matrices. The pressure effects were measured at 6 K in He gas compressed up to 200 bar. The analysis of pressure shifts is simpler than the interpretation of thermal effects that are inevitably complicated by a volume change. Thus, the baric studies are in a sense ''cleaner''. Based on the pressure-shift data, pure thermal shifts could be uncovered, and their frequency dependence compared with the predictions of the model. The available pressure shifts of narrow holes in the protein spectra (15–17) are reconsidered from the point of view of realistic interaction potentials that include repulsive, dispersive, and electrostatic forces. A comparison of the properties of the holes and the broadband spectra is carried out in the last section. A new effect, a narrowing of inhomogeneous bandwidth as a result of thermal expansion is predicted and confirmed. Vibronic coupling effects are separated from the temperature-dependent inhomogeneous broadening.

MATERIALS AND METHODS

The pigments 1,8-diphenyloctatetraene, β-carotene (see Fig. 1 for abbreviations and chemical structures), and the polymers were purchased from Aldrich (Milwaukee, WI), chlorophyll a (Chl a) was obtained from Serva (Heidelberg, Germany). Chlorin was available from our previous studies (18). Pheophytin a was prepared from Chl a by adding a drop of 10 M HCl to a solution in acetone/water. Photosystem II CP47-RC (CP47-D1-D2-cytochrome b-559) complexes were prepared from spinach grana membranes using n-dodecyl-β,D-maltoside (DM), and served as starting material for the isolation of the CP47 complex using a LiClO$_4$/DM treatment (19). For low-temperature measurements, the samples were diluted in BTT buffer (20 mM BisTris, 20 mM NaCl, 10 mM MgCl$_2$, 1.5% taurine, pH 6.5) supplemented with 0.03% DM and 70% (v/v) glycerol (20).

The samples were cooled either in a He-flow cryostat CF 1204 or a liquid-nitrogen reservoir cryostat DN 1704 (Oxford Instruments, Oxford, UK), and the temperature was maintained within 1° with the Oxford ITC-4 temperature controller. Absorption spectra were recorded on a Lambda 9 spectrophotometer (Perkin-Elmer, Wellesley, MA) with 1-nm slit width or a computer-controlled Cary 219 spectrophotometer (slit width 0.5–1 nm, scan speed 0.5 nm/s). Wavelength calibration was performed versus the 416.1-, 536.5-, and 640.5-nm lines of HoCl$_3$ (0.25 M in 10 mM HCl). The reproducibility was better than 0.05 nm and corrections did not exceed 0.3 nm. The spectra are displayed and analyzed as measured, with no correction for instrumental slit width and refractive index of air.

Spectral holes were burned with an LPD 3002E dye laser, pumped with 308 nm light from an LPX 100 excimer laser (Lambda Physik, Göttingen, Germany). Holes were detected in transmission by scanning the dye laser with attenuated energy at 40 Hz pulse frequency, using a two-channel set-
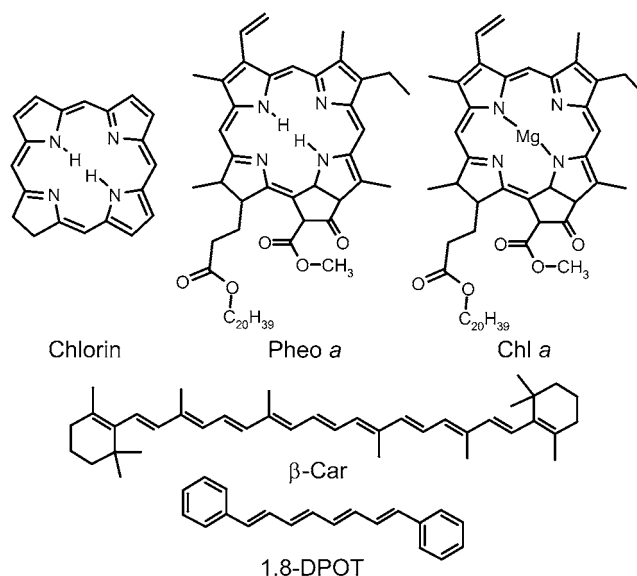
FIGURE 1   Chemical structures of pigments.

up of a Coherent-Molectron JD2000 joulemeter/ratiometer (Santa Clara, CA). The sensitive J3S-10 (10^9 V/J) probe was placed in the sample channel and the less sensitive one, J3-09 (10^3 V/J) served to measure the laser pulse energy. Pressure studies were carried out in a cylindrical cell of 20 mm in diameter, made of stainless steel and supplied with two sapphire windows. A piece of polymer film was placed in a sample volume of $2 \times 4 \times 4$ mm^3 that was filled with gaseous He at 200 bar and cooled down to 6 K, and the holes were burned. Subsequently, the pressure was released step by step and the holes were recorded. Temperature (T) and pressure (P) effects were investigated on deep holes burned at different positions of the inhomogeneous band at low T (5–7 K). Deep holes were created to improve the line/background ratio, so that the hole width exceeded the quasihomogeneous value by a factor of 2–4.

INTERMOLECULAR POTENTIALS AND THE SPECTRA

Sharp lines are usually transformed to broad phonon bands if atoms are embedded in a rare-gas solid (21). In molecules, vibrations and rotations add to the immense complexity of spectra. Thus, the observation of narrow resonant transitions of large aromatic molecules in frozen n-alkane solvents, or the so-called Shpol'skii systems, was totally unexpected (22). The concept of ZPLs in the optical impurity spectra in solids, including polymers and proteins, became firmly rooted only after the discovery of site-selection and hole-burning methods two decades later (23,24). As a result of inhomogeneous broadening, the ZPLs are hidden in glasses and the spectra remain broad, even at 0 K. Complete interpretation of spectra is a daunting task requiring a microscopic description of the environment, in addition to detailed knowledge of interparticle potentials in both the initial and final electronic states. However, it is possible to reproduce many interesting properties of inhomogeneous distribution and ZPLs in terms of effective two-body potentials (25,26).

The potential energy of a spherical impurity molecule surrounded by i (spherical) matrix particles may be written as a sum of pairwise interactions of a power series having j members:

$$U_g = \Sigma_i \Sigma_j a_{mj} r_i^{-mj}, \qquad (1)$$

where r denotes the distance, and a_m the constants that can have different signs (a negative sign corresponds to attractive interaction). The power coefficients can be assigned to interaction mechanisms, e.g., $m = 1, 3, 6,$ and 12 stands for Coulombic, dipole-dipole, dispersive, and exchange interactions, respectively.

A realistic potential must possess a steep ascending branch at close distances, a dissociation limit, and must display a minimum at the equilibrium coordinate. Disorder in noncrystalline solids means that not all particles can occupy a potential minimum. As a consequence, structural relaxation is always occurring in glasses. However, at temperatures considerably below the glass point, T_g, the relaxation is exponentially slow, and the global minimum can never be reached. The relaxation is also very limited after optical excitation. The coefficients a_{mj} will change in the excited state, and the optical transition energy in vacuum ν_0 is added to the potential:

$$U^* = \Sigma_i \Sigma_j a_{mj}^* r_i^{-mj} + \nu_0. \qquad (2)$$

The optical transition energy ν can be expressed as a difference between the potentials of excited and ground states, U^* and U_g, respectively (Fig. 2, *vertical arrows*). Absolute solvent shift $\Delta\nu$ with respect to transition energy of the free chromophore ν_0 amounts to

$$\Delta\nu = \nu - \nu_0 = U^* - U_g - \nu_0. \qquad (3)$$

The structure of a guest-host system is established at the glass temperature, T_g, so that the spread of solvation energies is in the order of thermal energy, $k_B T_g$. The Boltzmann distribution can be written as (Fig. 2)

$$\Phi = \exp(-U_g/k_B T_g). \qquad (4)$$

Spectral distribution of zero-phonon transitions is obtained by plotting Φ against the solvent shift $\Delta\nu$ (Eq. 3).

Pressure-shift coefficients of spectral lines within the inhomogeneous band can be expressed as differences in the first derivatives that may be drawn also as a function of $\Delta\nu$, rather than r:

$$d\nu/dP = -\alpha_T r(d(U^* - U_g)/dr) = -\alpha_T r \Delta U', \qquad (5)$$

where α_T is linear isothermal compressibility ($\alpha_T = -(dr/dP)_T/r$).

The line broadening and shift above 0 K are of dynamic origin (9,10). Broadening depends on the dynamic modulation of electronic energy levels by matrix fluctuations, whereas the shift arises as a result of a phonon frequency change, accompanying optical excitation. In the case of a weak
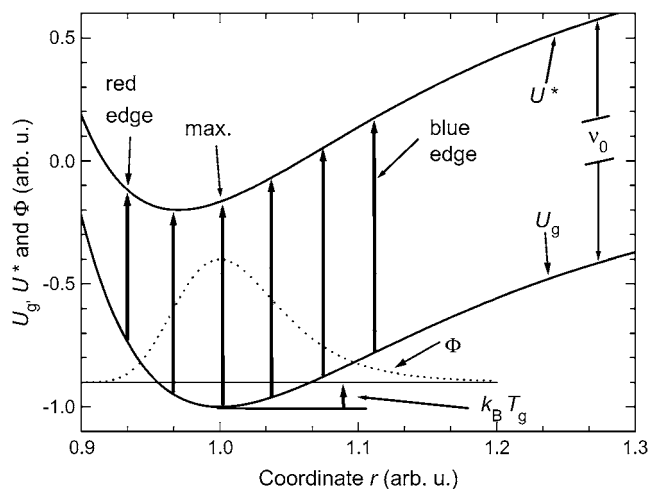

FIGURE 2 Optical transitions from the ground-state potential surface (U_g) to excited level (U^*) (*bold arrows*); ν_0 is the transition energy of nonsolvated chromophore. Dotted curve is the Boltzmann distribution of solvation energies for thermal energy at the glass transition $k_B T_g$, equal to one-tenth of the potential well depth in the ground state (Eq. 4).

interaction with a single harmonic pseudolocal mode, the nonperturbative QEPC theory yields the following expressions for line shift, ν_T, and homogeneous line width, Γ_h (in frequency units) (9,10):

$$\nu_T = \frac{1}{2}W\omega_g n(\omega_g); \qquad (6)$$

$$\Gamma_h = \frac{1}{4}W^2 \omega_g^2 \tau_g n(\omega_g)(n(\omega_g) + 1), \qquad (7)$$

where W denotes the QEPC constant, ω_g is the phonon frequency in the ground state, τ_g is the lifetime of the phonon level, and $n(\omega_g)$ is the Bose factor ($n(\omega_g) = (\exp(h\omega_g/k_B T) - 1)^{-1}$). Very similar formulas apply for an optical Einstein mode, where phonon bandwidth is introduced instead of the lifetime (10).

The QEPC constant depends on harmonic frequencies in the ground (S_0) and excited (S_1) state (ω^*):

$$W = (\omega^*/\omega_g)^2 - 1. \qquad (8)$$

The QEPC constant W characterizes the difference in curvatures of potential energy surfaces for a (pseudo)local vibration in the ground and excited electronic states of a chromophore. The second derivative of a potential function yields the force constant k:

$$k = d^2U/dr^2 \equiv U''. \qquad (9)$$

The corresponding harmonic frequency can be written as

$$\omega = (2\pi)^{-1}(k/\mu)^{1/2}, \qquad (10)$$

where μ is reduced mass. Consequently, W can be written as $U^{*\prime\prime}/U_g'' - 1$.

Strictly speaking, potentials (Eqs. 1 and 2) can hardly be treated as dynamical variables, since in a very slowly relaxing glass the forces between any pair of particles are

compensated in the sense of Newton's Third Law, and the first derivative does not define a condition of mechanical equilibrium. In fact, disorder in glasses can only be maintained by multibody interactions between the molecules. However, if the roughness of a potential hypersurface responsible for metastability would suddenly disappear, a relaxation sets in, driven by a force $-dU/dr$. Without any doubt, the presence of voids in the lattice can lead to the localization of phonons. A larger free volume probably corresponds to a more extensive softening of the modes localized nearby. As a result, a single coordinate model can be physically insightful, as far as the vibrational dynamics in glasses is concerned (25,26).

The proposed model will be illustrated for simple Lennard-Jones (L-J) 6-12 potentials, representing exchange repulsion and London (dispersion) forces:

$$U_{\mathrm{g}} = \varepsilon_{\mathrm{g}}((\sigma_{\mathrm{g}}/r)^{12} - 2(\sigma_{\mathrm{g}}/r)^6), \tag{11}$$

where ε_{g} is the depth and σ_{g} is the position of potential minimum in the ground-state equilibrium. To relate the energy distribution of the ground state Φ (Eq. 4) to inhomogeneous distribution function (IDF) of optical transition energies, the parameters of the excited state, ε^* and σ^*, should be introduced:

$$U^* = \varepsilon^*((\sigma^*/r)^{12} - 2(\sigma^*/r)^6) + \nu_0. \tag{12}$$

If a transition is subject to a negative (red or bathochromic) vacuum-to-matrix shift, the potential well is expected to be deeper in the excited state. According to London formula,

the relative well depth, $\varepsilon^*/\varepsilon_{\mathrm{g}}$, should be close to the ratio of polarizabilities in the excited and the ground states, $\alpha^*/\alpha_{\mathrm{g}}$, and depend on the slope of a solvatochromic plot in nonpolar solvents p ($p < 0$, Table 1) (12,26):

$$\varepsilon^*/\varepsilon_{\mathrm{g}} = \alpha^*/\alpha_{\mathrm{g}} = 1 - 1.8 \times 10^{-4} p. \tag{13}$$

Fig. 3 a shows the calculated inhomogeneous bands having different solvent shifts, or relative well depths, $\varepsilon^*/\varepsilon_{\mathrm{g}}$, ranging from 1.2 to 2 (with p varying between -1000 and -5000 cm^{-1}). The ground-state distribution, Φ (Eq. 4, Fig. 2), was obtained for thermal energy equal to one-tenth of well depth ($\varepsilon_{\mathrm{g}}/k_{\mathrm{B}}T = 10$). The peak of Φ (and IDF) is normalized at the ground-state minimum by adding ε_{g} to the numerator in Eq. 4. A small displacement of potential minima by 1% effectively removes the degeneracy in optical transition energies (25,26). The IDF is symmetrical and nearly Gaussian, if $\sigma^*/\sigma_{\mathrm{g}}$ scales to $(\varepsilon^*/\varepsilon_{\mathrm{g}})^{-1/12}$ (Fig. 3). The band broadens fast with decreasing $\sigma^*/\sigma_{\mathrm{g}}$, and develops a shallow slope of the red flank, if $\sigma^*/\sigma_{\mathrm{g}}$ is $(\varepsilon^*/\varepsilon_{\mathrm{g}})^{-1/6}$ or less (26).

The pressure (P) effect on IDF can easily be obtained if the compression is hydrostatic and isotropic, and all interparticle distances scale by the same factor of b. The potential energy of the ground state is changed to

$$U'_{\mathrm{g}(P)} = \varepsilon_{\mathrm{g}}((b\sigma_{\mathrm{g}}/r)^{12} - 2(b\sigma_{\mathrm{g}}/r)^6). \tag{14}$$

Besides shifting to shorter distances, the distribution width of ground-state energies (Eq. 4) is actually shrinking on compression. However, the IDF broadens with increasing P, since

TABLE 1   Temperature dependence of absorption band maxima of pigments in polymers and proteins

Pigment	Transition	Matrix	ν_0(cm^{-1})	$\nu_{\max}$, 0 K(cm^{-1})	$\Delta\nu_{\max}$, 0 K(cm^{-1})	p(cm^{-1})	$d\nu_{\max}/dP$ (GHz/bar)	$\Delta\nu_{\mathrm{obs}}$, 293 K(cm^{-1})	ν_{solv}, 293 K (cm^{-1})*	ν_{T}, 293 K (cm^{-1})
Chlorin	S$_1$	PMMA	15,912(j)	15,814.3 ± 0.5	−98	−659 ± 20	−0.121	−74	11	−85
Pheo a	S$_1$	PVB	15,173 ± 8	15,011 ± 2	−162	−980 ± 30	(−0.18)	−61 ± 2	15	−77
	S$_2$	PVB	19,080 ± 20	18,657 ± 4	−423	−1480 ± 80	(−0.27)	−50 ± 4	23	−76
	Soret	PVB	25,400 ± 60	24,146 ± 10	−1254	−4300 ± 250	(−0.84)	28 ± 10	72	−44
Chl a	S$_1$	PVB	15,550 ± 50	15,032 ± 4	−518	−1700 ± 150	(−0.32)	−30 ± 4	27	−57
	S$_1$	CP47		14,825 ± 5	−725			(4)[†]	54	−51
Chl a	Soret	PVB	24,000 ± 200	22,966 ± 8	−1034	−3300 ± 500	(−0.64)	40 ± 10	54	(−14)[†]
	Soret	CP47		22,823 ± 8	−1177			62	106	(−46)[†]
β-carotene	S$_{21}$	PMMA	24,260 ± 180	21,627 ± 10	−2630	−9000 ± 700	(−1.77)	86	152	−67
	S$_{21}$	PS		21,190 ± 10	−3070			170 ± 15	138	(20)[†]
	S$_{20}$	CP47	22,780 ± 180	19,930 ± 10	−2840			360 ± 20	297	(64)[†]
1,8-DPOT	S$_{20}$	PMMA	27,732 ± 40	24,709 ± 3	−3023	−10,024 ± 166	(−1.97)	183	171	12

ν_0, 0-0 transition energy in vacuum, measured in a cold jet (j (27)) or extrapolated from solvent shift data (20,28,29); $\nu_{\max}$, absorption-band maximum measured at 6 or 77 K and extrapolated to 0 K; $\Delta\nu_{\max}$, solvent shift $\nu_{\max} - \nu_0$; p, steepness of a plot of band maxima in liquid n-alkanes at 293 K versus the Lorentz-Lorenz function (polarizability) of solvents (20); $d\nu_{\max}/dP$, pressure-shift coefficient of a spectral hole burned at the band maximum (18), with values in parentheses estimated from Eq. 19; $\Delta\nu_{\mathrm{obs}}$, temperature shift between 0 and 293 K; ν_{solv}, solvent shift component of thermal shift $\Delta\nu_{\mathrm{obs}}$ at 293 K; ν_{T}, pure thermal, phonon-induced shift of band maxima at 293 K.
*ν_{solv} was calculated from Eq. 20 using the following isochors: $P_{\mathrm{V}} = -14 + 0.307T^{1.591}$ for PMMA and PVB; $P_{\mathrm{V}} = 3.97T^{1.23}$ for PS; and that of the PEld $P_{\mathrm{V}} = -9.7T + 2.85T^{1.395}$ (26) was used for CP47.
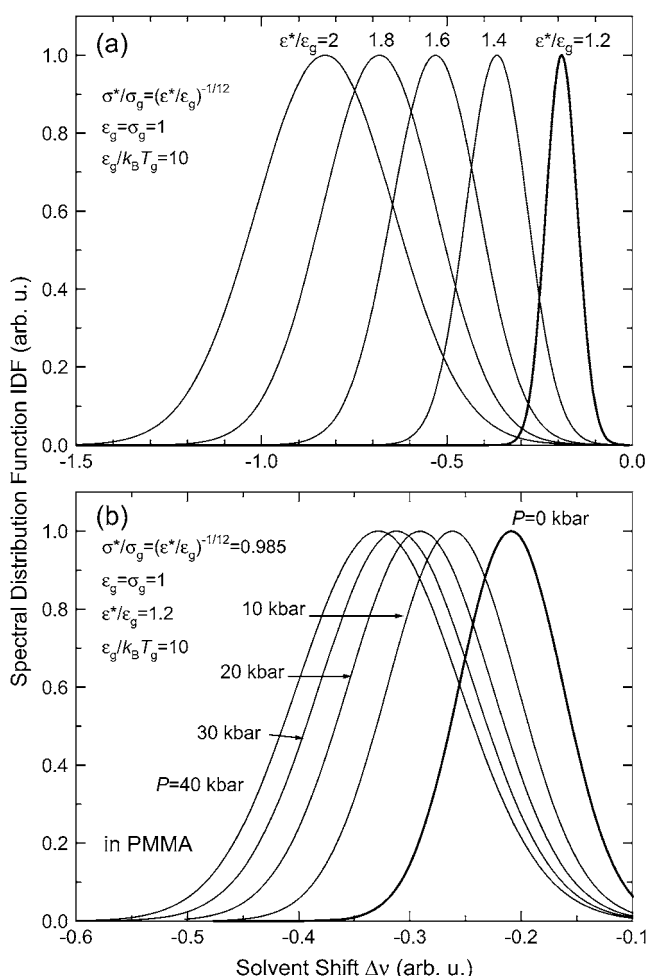[†]U-shaped T dependence.

FIGURE 3 (a) Inhomogeneous bands at different relative depths of potential minima, $\varepsilon^*/\varepsilon_g$, calculated from the Boltzmann distribution of solvation energies for a Lennard-Jones potential with $\varepsilon_g = \sigma_g = 1$ (Eq. 4), and plotted versus the solvent shift (Eq. 3). The relative equilibrium position of excited state σ^*/σ_g was scaled to as $(\varepsilon^*/\varepsilon_g)^{-1/12}$. (b) Pressure broadening and shift of IDF for $\varepsilon^*/\varepsilon_g = 1.2$ (shown on a different scale also in a), in a host matrix with isothermal compressibility equal to that of PMMA (30).

the solvent shift has a steep distance dependence for $\sigma^*/\sigma_g < 0.99$ (25).

The broadening and bathochromic shift at P up to 40 kbar are illustrated in Fig. 3 b for a matrix with the compressibility of poly(methyl methacrylate) (PMMA) (30). The behavior of S_1 bands of anthracene and phenanthene in the PMMA matrix (31) compares well with the predictions of the model if the ratio of equilibrium distances σ^*/σ_g is slightly less than unity ($\sim(\varepsilon^*/\varepsilon_g)^{-1/12}$). Baric blue shifts almost never occur in organic systems, even at the highest pressure (31), although it may seem that a rapid increase of repulsive forces should up-shift transition energy. Indeed, if the equilibrium coordinates coincide in the upper and lower states ($\sigma^* = \sigma_g$), the negative solvent shift would diminish under pressure (25). It is important to keep in mind that at least 90% of the solvent shift is generated in the first layer of solvent molecules that

are in van der Waals contact with the chromophore (32). Thus, the concept of the pressure shift as a continuation of solvent shift cannot be saved by assuming that the red shift on compression originates from bringing closer outer coordination shells that are much less affected by repulsive potentials. Therefore, the equilibrium coordinate of the excited-state potential σ^* should indeed be $<\sigma_g$. A careful analysis of inhomogeneous band shapes and their transformation under pressure is needed for establishing the size of effective interacting units (either atoms, groups of atoms, whole solvent molecules, or monomeric units in the case of polymers), and the subsequent determination the potential functions for chromophores in different electronic states.

Barochromism at high pressures has been investigated previously (31) and will not be elaborated further. Instead, pressure shifts of narrow spectral holes burned at different frequencies over the inhomogeneous band will be discussed. The pressure-shift coefficients are obtained by differentiation of the solvent shift (Eq. 5):

$$d\nu/dP = 4\beta_T[\varepsilon^*(\sigma^*/r)^{12} - \varepsilon^*(\sigma^*/r)^6$$
$$- \varepsilon_g(\sigma_g/r)^{12} + \varepsilon_g(\sigma_g/r)^6], \qquad (15)$$

where β_T is isothermal bulk compressibility ($\beta_T = 3\alpha_T$).

In the vicinity of band maximum ($r = \sigma_g$), for a slope of the plot of $d\nu/dP$ versus the frequency (25), one obtains

$$a_{max} = 2\beta_T(2(\sigma^*/\sigma_g)^{12} - (\sigma^*/\sigma_g)^6 - \varepsilon_g/\varepsilon^*)/$$
$$((\sigma^*/\sigma_g)^{12} - (\sigma^*/\sigma_g)^6)). \qquad (16)$$

If the ratio of the relative shifts of potential minima $\varepsilon_g/\varepsilon^*$ scales either as $(\sigma^*/\sigma_g)^{12}$ or $(\sigma^*/\sigma_g)^6$, the slope values of $2\beta_T$ and $4\beta_T$ follow from Eq. 16. A numerical example with $\varepsilon^*/\varepsilon_g = 1.2$ shows that the pressure shift coefficients are linear over a wide range of solvent shifts for a displaced potential well minimum, with σ_g/σ^* equal to either 0.97 ($(\varepsilon^*/\varepsilon_g)^{-1/6}$) or 0.985 ($(\varepsilon^*/\varepsilon_g)^{-1/12}$) (Fig. 4). The slopes varying between $2\beta_T$ and $4\beta_T$, as well as the sign of deviations of $\nu_{0(P)}$ ($\nu_{0(P)}$ is the frequency where no P shift occurs) from ν_0 agree well with the P shifts of spectral holes in polymers (18) and ethanol glass (28).

In terms of L-J potentials, the QEPC constant can be expressed as (Eqs. 8–10):

$$W = U^{*\prime\prime}/U_g{}^{\prime\prime} - 1$$
$$= (\varepsilon^*(13(\sigma^*/r)^{12} - 7(\sigma^*/r)^6)/$$
$$\varepsilon_g(13(\sigma_g/r)^{12} - 7(\sigma_g/r)^6)) - 1. \qquad (17)$$

In Fig. 4, W is plotted versus the solvent shift. If the minima are not shifted, the QEPC constant at the band maximum ($r = \sigma_g = \sigma^*$) would depend only on the relative depth of potential wells as $\varepsilon^*/\varepsilon_g - 1$. For $\varepsilon^*/\varepsilon_g = 1.2$, the solvent shift at the band maximum is ~-0.2, and the thermal shift would be toward higher frequencies, since W is positive (0.2). Therefore, thermal blue shifts would be predicted for
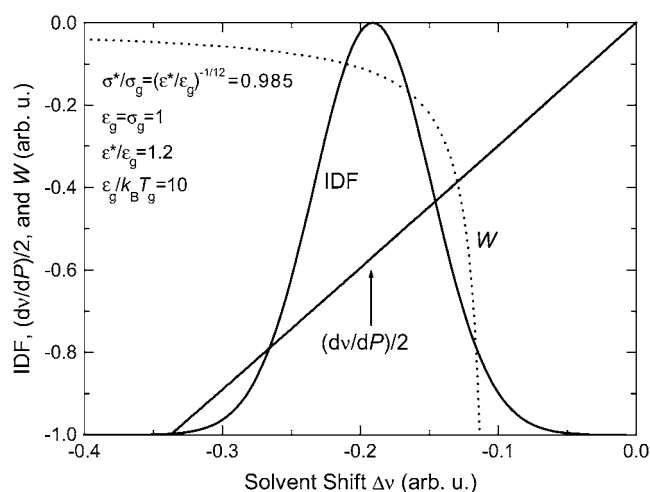
FIGURE 4 Calculated solvent shift dependencies at a displacement of potential minima σ^*/σ_g equal to $(\varepsilon^*/\varepsilon_g)^{-1/12}$ (0.985) for pressure-shift coefficients $d\nu/dP$ (multiplied by 0.5, *solid straight line*), and QEPC constant W (*dotted line*). Inhomogeneous band shape was calculated as described in Fig. 3.
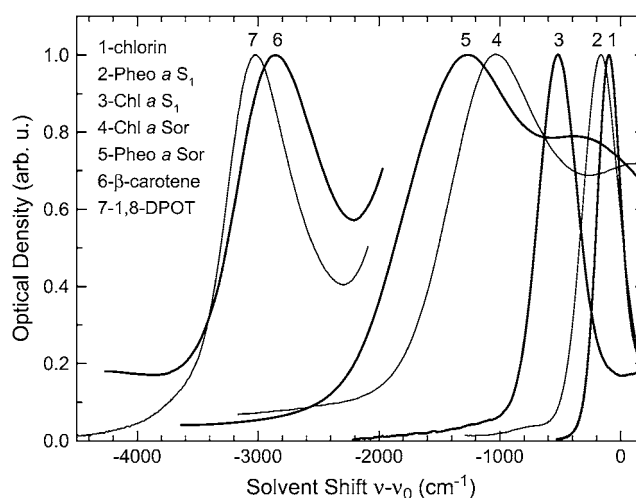

FIGURE 5 Normalized absorption spectra of tetrapyrrolic pigments chlorin, pheophytin *a*, and chlorophyll *a* (*1–5*) and polyenic chromophores (*6* and *7*), shown on the scale of absolute solvent shift (see Table 2). Chlorin (*1*) and 1,8-diphenyloctatetraene (*7*) were measured in PMMA at 6 K, pheophytin *a* (*2* and *5*) and chlorophyll *a* (*3* and *4*) in PVB at 80 K, and β-carotene in pigment-protein CP47 at 80 K.

transitions with red (negative) solvent shifts, contrary to observations. When the potential wells are shifted, having $\sigma^*/\sigma_g < 0.985$, bathochromic shifts are obtained ($W < 0$). Moreover, a diminishing of thermal red shifts when moving toward the low-frequency edge is evident (Fig. 4), in agreement with the behavior of spectral holes.

RESULTS AND DISCUSSION

Absorption spectra

Complicated absorption contours are sometimes deconvoluted to multiple Gaussians (33) or, alternatively, analyzed by the method of moments (34), often with ambiguous results. A nondegenerate transition that is well separated from other electronic and strong vibronic bands is simpler to analyze at low temperature (6 K or even 77 K (Fig. 5)), because QEPC vanishes in the low-temperature range, so that the observed contour depends solely on the shapes of the IDF and the phonon side band.

Thermal shift of band maxima

It has been recognized for some time that the spectral shifts have, besides QEPC, a density-dependent component (13,14,20). The shifts caused by thermal expansion were estimated on the basis of pressure-shift coefficients of spectral holes burned at the band maxima, $d\nu_{max}/dP$, and "thermal pressure", P_V, derived from the isochore equation

$$P_V = \int_0^T (\alpha_P/\alpha_T)dT. \tag{18}$$

The accurate isobaric thermal-expansion coefficients, α_P, are available in a broad temperature range for PMMA (35) and polyethylene (36). Linear compressibility, α_T, of

polymers shows weak temperature dependence (37). Thermal volume expansion of PMMA amounts to 3.7% at room temperature, and the shrinking on cooling from 293 K to 0 K is equivalent to a compression by 2.6 kbar at 293 K. Pressure-shift coefficients, $d\nu_{max}/dP$, are available for a number of chromophores (18,28). For the remaining compounds, $d\nu_{max}/dP$ can be estimated from a correlation with the slope of solvatochromic plots p (Table 1):

$$d\nu_{max}/dP(\text{GHz/bar})$$
$$= (0.020 \pm 0.06) + (1.99 \pm 0.30) \times 10^{-4} p(\text{cm}^{-1});$$
$$R = 0.937, n = 8. \tag{19}$$

Multiplication of $d\nu_{max}/dP$ by $-P_V$ gives the solvent shift that is to be subtracted from the observed hole shift, $\Delta\nu_{obs}$, to obtain the pure thermal, phonon-induced shift, ν_T (Table 1):

$$\nu_T = \Delta\nu_{obs} - (d\nu_{max}/dP)P_V. \tag{20}$$

The observed shifts of band maxima vary widely in sign and magnitude between 6 K and 293 K (Fig. 6), from −74 cm^{-1} in chlorin to 183 cm^{-1} in 1,8-diphenyloctatetraene (1,8-DPOT) in PMMA (Fig. 7 *a*). Similar to 1,8-DPOT, the spectrum of β-carotene at 293 K is subject to a large hypsochromic displacement by 86 cm^{-1} in PMMA, 170 cm^{-1} in poly(vinyl butyral) (PVB), and 360 cm^{-1} in CP47 (Fig. 8). It turns out, however, that all blue shifts are caused by a decrease in solvent shifts as a result of matrix expansion. Pure thermal shifts are bathochromic, with the exception of 1,8-DPOT that has ν_T at almost zero over the whole temperature range (Fig. 7 *b*). Remarkably, the temperature dependence of ν_T shows sometimes an upward curvature (particularly for β-carotene in CP47), leading to a diminishing
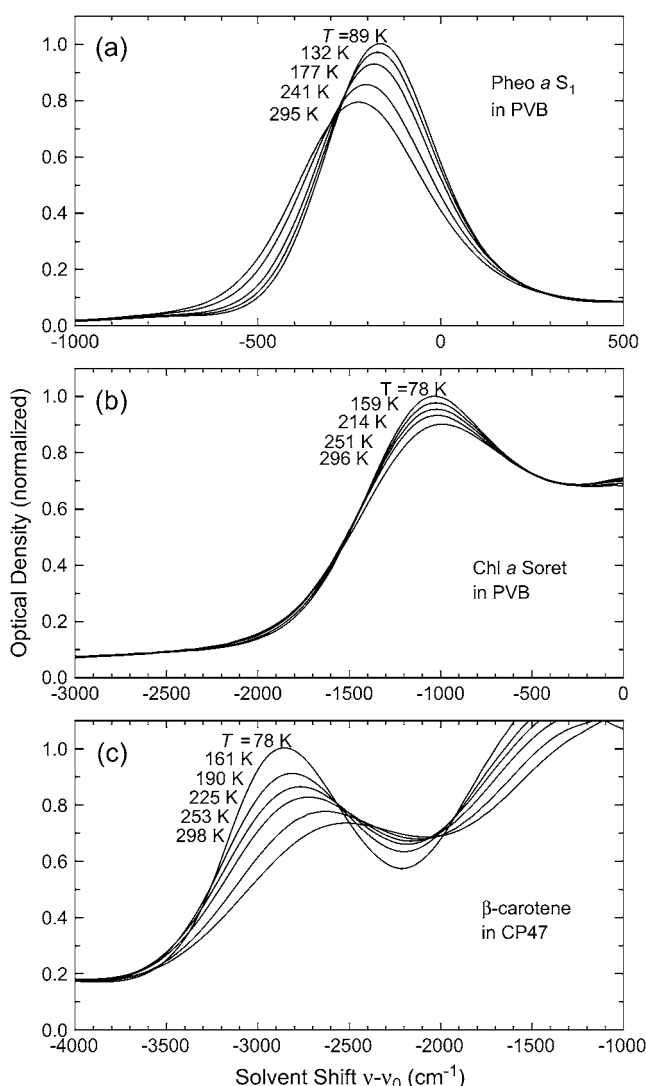
FIGURE 6 Temperature dependence of (*a*) S_1 (Q_y) absorption of pheophytin *a* and (*b*) Soret band of chlorophyll *a*, both in poly(vinyl butyral) films, and (*c*) S_{20} ($1^1B_u \leftarrow 1^1A_g$) band of β-carotene in chlorophyll-protein CP47.

FIGURE 7 (*a*) Observed temperature-induced shifts of absorption maxima and (*b*) phonon-induced shift component ν_T for chlorin, β-carotene, 1,8-DPOT (in PMMA), pheophytin *a*, and chlorophyll *a* (in PVB). The ν_T was obtained as a difference between the observed shift and solvent shift due to thermal expansion (Eq. 20).

of the negative shift at higher temperature (Figs. 7 *b* and 8). One can speculate that certain internal modes, having higher frequencies than the matrix phonons, become more rigid in the excited state, and give rise to a positive *W* and a hypsochromic shift. Otherwise, low-frequency, pseudolocal vibrations universally produce red shifts.

Therefore, in the host-guest systems under study, the observed solvent shifts at 0 K and the phonon-induced displacements are both bathochromic. Negative thermal shift may seem incompatible with a vacuum-to-matrix shift of the same sign, since the latter presupposes a stabilization of the excited state. This, in turn, would correspond to a steeper potential well, which is characterized by higher vibrational frequencies. Mode stiffening in the excited state translates to a positive coupling constant *W* (Eq. 8). This paradox can
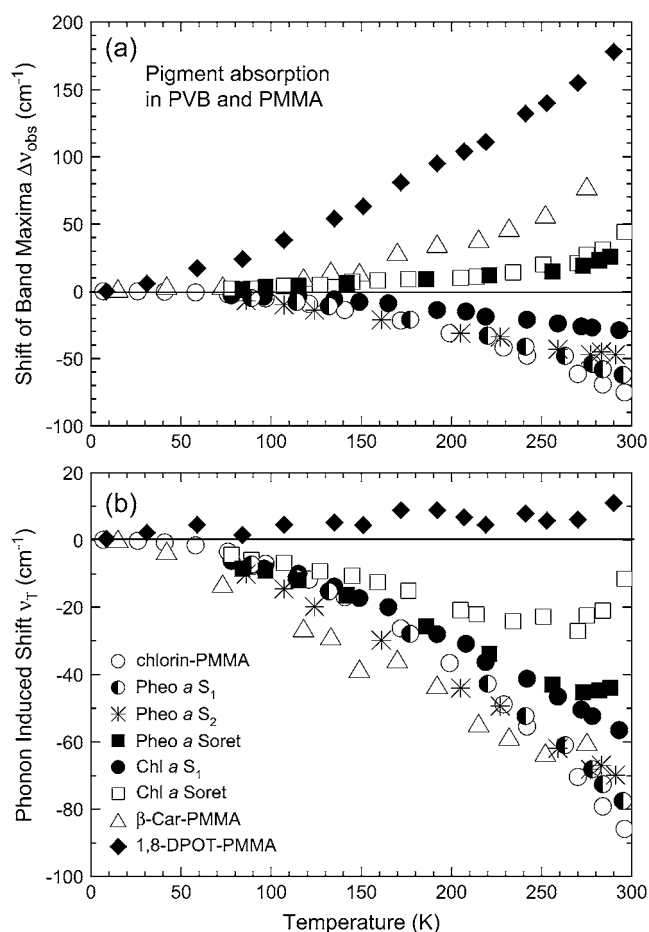
be resolved if the equilibrium distance is shorter in the excited state ($\sigma^* < \sigma_g$ (Fig. 4)).

Thermal broadening

As expected, the bandwidths (double half-widths at half-maximum (2hwhm)), which vary between 230 and 1200 cm^{-1} (Table 2), follow roughly the absolute solvent shifts, $\Delta\nu_{max}$ (Fig. 3 *a*), spanning from −100 to −3000 cm^{-1} (Table 1). Large deviations from the proportionality between the bandwidth and the solvent shift point either to a strong linear vibronic coupling or additional inhomogeneous broadening caused by electrostatic interactions (38) (also Fig. 6 of Renge (28)).

The shape of the IDF can be determined from a distribution of the saturated depths of spectral holes or, alternatively, by recording intensities of a well-defined vibronic fluorescence line while exciting within the 0-0 band by laser (38–40). IDF is difficult to measure accurately if the ZPLs are either weak or broad, as in the Soret bands of porphyrins
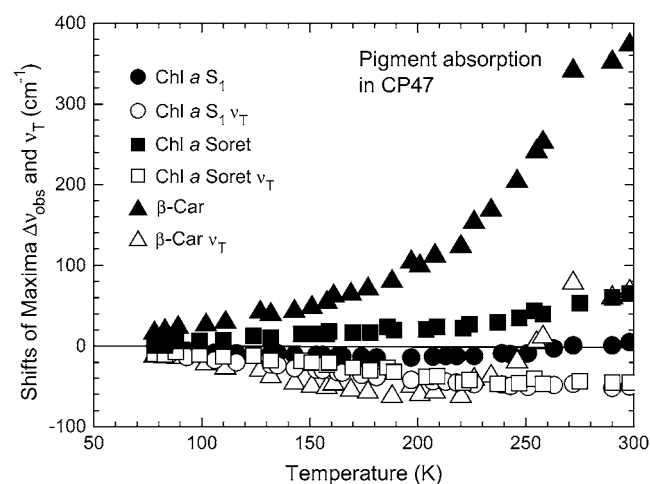
FIGURE 8 Temperature-induced shifts of absorption maxima (*solid symbols*) and the respective pure thermal, phonon-induced component ν_T (*open symbols*) for the S_1 and Soret transitions of chlorophyll *a*, and the S_{20} band of β-carotene in chlorophyll-protein CP47.

or the S_2 bands of polyenes. In the case of higher transitions the excitation profiles of coherent anti-Stokes Raman scattering may offer an approach to inhomogeneous broadening (41). On the other hand, the red flanks of 0-0 bands roughly coincide with IDF, provided that less than a few low-frequency phonons with ν_{ph} of 10–30 cm^{-1} are created (42). This condition is met for many S_1 transitions in tetrapyrroles and polyarenes, where the Huang-Rhys factor S is <1 (the Debye-Waller factor (DWF) α, equal to e^{-S}, is >0.37) (43).

Most absorption bands (Fig. 5) can be approximated very well to Voigt profiles in the whole temperature range. The Voigtian treatment yields the widths of a Gaussian (Γ_G), representing a steep, exponential fall-off, and a Lorentzian (Γ_L) that has a shallow, hyperbolic tail. Because of asymmetry, the spectra were cut on the blue flank at 90% or 95% of maximum height, and the low-frequency part, including the peak, was subject to fitting. A large Γ_G/Γ_L ratio points to a prevalence of Gaussian shape in the S_1 bands of

chlorin ($\Gamma_G/\Gamma_L = 7.3$) and Pheo *a* (($\Gamma_G/\Gamma_L = 5.3$) (Table 2). An appreciable Lorentz contribution to S_1 ($\Gamma_G/\Gamma_L = 2.3$) and Soret bands ($\Gamma_G/\Gamma_L = 2.9$) of Chl *a* indicates that spectra fall off less steeply than the exponential law. Thermal broadening renders the S_1 and S_2 spectra of porphyrins closer to a Lorentzian (Figs. 6 *a* and 9), as shown by a decrease of the Γ_G/Γ_L ratio at room temperature (Table 2). In contrast, the broadening of Soret transitions in Pheo *a* and Chl *a* is predominately Gaussian. It is quite distinctive that the S_{20} band of β-carotene in CP47 protein complex is a nearly perfect Gaussian 691 cm^{-1} wide at 80 K, and retains its shape at room temperature, albeit reaching the width of 1196 cm^{-1} (Fig. 6 *c*). Severe vibronic congestion of the S_2 band system of β-carotene complicates the band shape analysis in polymers, but it is still obvious that deviations from a Gaussian contour are small.

Spectral hole burning

Hole burning in the spectra of chlorophylls in frozen solvents dates back to 1981 (44,45), and was subsequently performed in situ on etiolated and greening leaves (46,47) and numerous pigment-protein complexes (48–50). The parent chlorin has stronger ZPLs and was chosen for hole burning in this work. The isocycle in Pheo *a* and the magnesium substitution in Chl *a* increase progressively the strength of linear EPC. The influence of pressure and temperature on spectral holes is illustrated in Fig. 10. The frequency dependencies (so-called color effects) of thermal and baric shifts and broadening are displayed together with the absorption contours of chlorin in PMMA and polyethylene (Fig. 11).

Pressure shift of spectral holes

Pressure-shift coefficients $d\nu/dP$ were determined at 6 K in two polymers with nearly identical volume compressibility (β_T), low-density polyethylene (PEld, $\beta_T = 1.41 \times 10^{-5}$ bar^{-1}) and PMMA ($\beta_T = 1.30 \times 10^{-5}$ bar^{-1}) (37). The slope of a linear plot of $d\nu/dP$ versus the burning frequency, denoted as a, is a function of matrix compressibility and the

TABLE 2 Temperature dependence of absorption bandwidths of pigments in polymers and proteins

Pigment	Transition	Matrix	2hwhm(Δ293 K) (cm^{-1})	Γ_G(Δ293 K) (cm^{-1})	Γ_L(Δ293 K) (cm^{-1})	Γ_G/Γ_L (293 K)	T dependence of 2hwhm
Chlorin	S_1	PMMA	229 ± 1 (38)	214 (−12)	29 (73)	7.30 (1.97)	$1.85 \times 10^{-6}T^{2.96}$
Pheo *a*	S_1	PVB	341 ± 2 (71)	304 (16)	57 (93)	5.3 (2.13)	$0.0114T^{1.54}$
Pheo *a*	S_2	PVB	368 ± 5* (75)	345 ± 5 (0)	42 (133)	8.2 (2.0)	$0.015T^{1.50}$
Pheo *a*	Soret	PVB	1155 ± 1* (204)	1084 (246)	90 (−60)	12 (44)	$0.015T^{1.68}$
Chl *a*	S_1	PVB	383 (54)	300 ± 5 (0)	132 (84)	2.3 (1.4)	$4.8 \times 10^{-4}T^{2.04}$
Chl *a*	Soret	PVB	895 (149)	746 (143)	260 ± 5 (10)	2.9 (3.3)	$1.5 \times 10^{-3}T^{2.02}$
β-carotene	S_{20}	PS	1162* (245)				$0.048T^{1.504}$*
	S_{20}	CP47	729 ± 5* (300)	691 (505)	0 (0)	∞ (∞)	$0.0086T^{1.84}$
1,8-DPOT	S_{20}	PMMA	577 ± 3 (248)	341 (227)	362 (75)	0.94 (1.3)	$0.0071T^{1.84}$

2hwhm, double value of the half-width at half-maximum on red side of the band, extrapolated to 0 K; Γ_G are Γ_L are the Gaussian and Lorentzian widths in a Voigt fitting of the low-frequency side of the spectrum, extrapolated to 0 K; the parameter value at 293 K or its change between 0 and 293 K are indicated in parentheses.
*Width of low-frequency band obtained by deconvolution of the whole vibronic contour to several Gaussians.
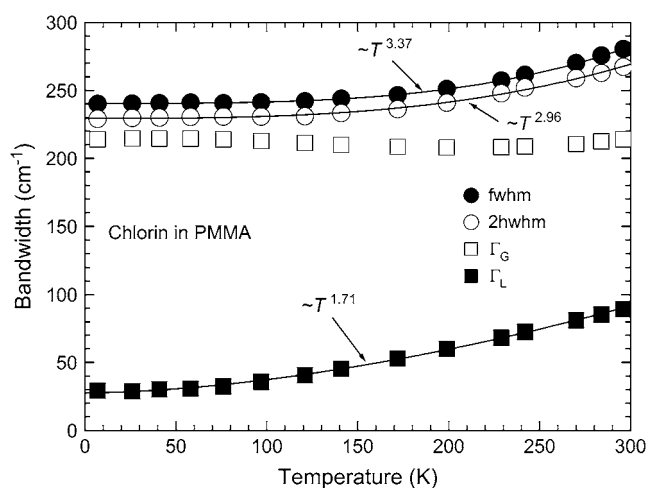
FIGURE 9 Temperature dependence of the bandwidths of chlorin S_1 absorption in PMMA: full-width at half-maximum (*fwhm, open circles*), double half-width at half-maximum (*2hwhm, solid circles*), and the respective Gaussian (Γ_G, *open squares*) and Lorentzian (Γ_L, *solid squares*) components of the Voigt fitting of the low-frequency half of the band. Temperature coefficients of a power-law fit are indicated.

power coefficients of interaction potential (Eq. 16). The slope a is steeper in PEld, $((4.38 \pm 0.12) \times 10^{-5} \text{ bar}^{-1})$, as compared to PMMA $((2.25 \pm 0.17) \times 10^{-5} \text{ bar}^{-1})$ (Fig. 11), or 9.3 and 5.1 times the linear compressibility, α_T ($\alpha_T = \beta_T/3$), respectively. When a single interaction type governs the solvent shift, the a to α_T ratio taken with a minus sign would give the power coefficient of a potential function (15,18). Unfortunately, a is not a constant depending solely on the host material, but varies within a factor of 3 for different dyes dissolved in PMMA (18) or ethanol glass (28). Moreover, the pressure shift vanishes at a frequency $\nu_{0(P)}$ that does not
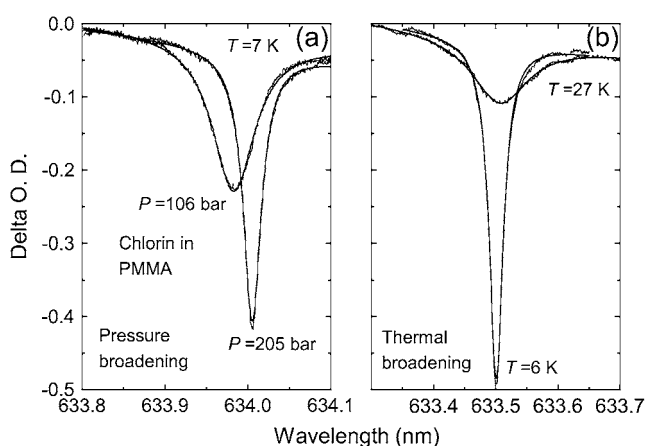
coincide with the 0-0 line of free chromophores in supersonic jets (Fig. 11). A steep pressure dependence ($a/\alpha_T = 9.3$) indicates that in PEld both dispersive and repulsive interactions with distance dependencies as r^{-6} and r^{-12} contribute to inhomogeneous broadening (Eq. 16). Electrostatic interactions can lower a in PMMA ($a/\alpha_T = 5.1$). The role of polar C-O groups of PMMA is also evident from a much broader bandwidth (230 cm^{-1}), as compared to nonpolar polyethylene (84 cm^{-1}) (Fig. 11).

The compressibilities, β_T, of a number of globular proteins can be remarkably small at room temperature ($(1 \pm 0.5) \times 10^{-5}$ bar^{-1}) (51), even less than those of polymers at cryogenic temperature, far below T_g, ranging between 0.8×10^{-5} and 1.8×10^{-5} bar^{-1} (37). Therefore, low magnitudes of β_T at 2 K, reported recently for bovine pancreatic trypsin inhibitor (16) and Zn-cytochrome c ($\sim 0.5 \times 10^{-5}$ bar^{-1}) (17) seem acceptable, although the authors have assumed a single power dependence of r^{-6}, neglecting the repulsive potential with r^{-12}. However, large inhomogeneous width in these systems points to electrostatic broadening mechanisms, plausibly with coefficients <6, which, by combining with a large repulsive coefficient, may result in an average of $\sim r^{-6}$, similar to chlorin-PMMA. On the other hand, the steep slopes within narrow spectral bands, with a varying from 6×10^{-5} to 8×10^{-5} bar^{-1}, which were assigned to β_T of 2×10^{-5} to 2.7×10^{-5} bar^{-1}, in horseradish peroxidase and myoglobin (52,53) (see also Table 5 in Renge (28) for a critical review of data), should originate mainly from the exchange repulsion, and cannot be regarded as evidence of

FIGURE 10 Broadening of spectral holes burned in the S_1 absorption of chlorin in PMMA accompanying a pressure or a temperature change. (*a*) Hole was burned at a He gas pressure of 205 bar, subsequently reduced to 106 bar, at $T = 7$ K. (*b*) Hole was burned at 6 K and then warmed up to 27 K. Hole shapes were approximated to Lorentzians, but the fit is poor in the case of pressure change that produces Gaussian broadening.
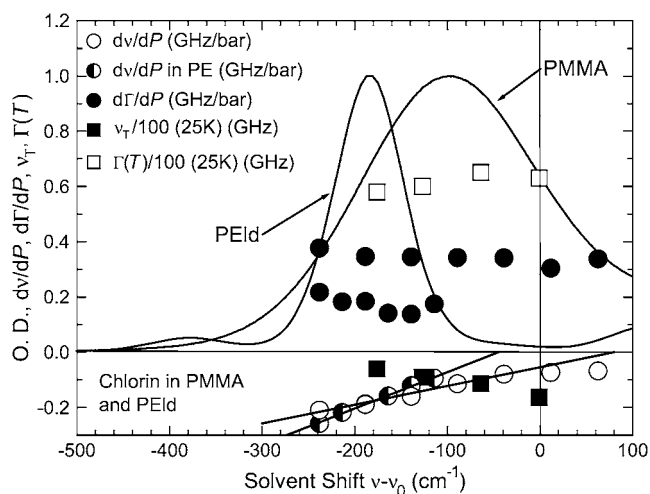

FIGURE 11 Normalized absorption spectra of chlorin in PMMA and PEld at 6 K, and the properties of spectral holes burned at different frequencies: coefficients of pressure shift (*dν/dP, open circles* and *half-shaded circles*) and broadening (*dΓ/dP, solid circles*) (the same symbol is used for PMMA and PEld), thermal broadening between 6 and 25 K ($\Gamma(T)$, *open squares*), and pure thermal shift at 25 K (ν_T, *solid squares*) (shown only for PMMA, in GHz units, divided by 100). The pressure shift in PEld and PMMA (*thick lines*) vanishes either below or above the 0-0 frequency of free pigment (15,912 cm^{-1} (27)), respectively.

high compressibility of these proteins. The determination of compressibility of host materials, including proteins, by means of pressure shifts of spectral holes could only be feasible if the mechanisms of inhomogeneous broadening are properly taken into account.

Pressure broadening of spectral holes

A pressure change in the He gas atmosphere surrounding the hole-burning sample, causes Gaussian broadening of initially Lorentzian hole shapes (Fig. 10 a). The amount of broadening was extracted by means of Voigtian deconvolution, by assuming that the Lorentz width remains constant. In contrast to baric shifts, the influence of the burning position on pressure broadening is weak (Fig. 11, *solid circles*). The broadening coefficients, $d\Gamma/dP$, tend to be larger at the band edges, sometimes forming a shallow U-shape (25,26,54). The two-body L-J model establishing a one-to-one relationship between the coordinate and the solvent shift cannot account for the hole broadening on a pressure change. Inasmuch as $d\nu/dP$ depends linearly on solvent shift (i.e., slope a is constant), the consideration of a larger number of particles than just two in the dispersive-repulsive potential model cannot lead to hole broadening on isotropic compression or dilatation. An important broadening mechanism could, therefore, derive from (multi)polar interactions.

Temperature shift of spectral holes

Recently, a prominent frequency dependence of thermal hole shifts has been established (25,26,54). The observed thermal shift, $\Delta\nu_{obs}$, is generally bathochromic, becoming less negative or slightly positive on the red edge of spectrum (Fig.
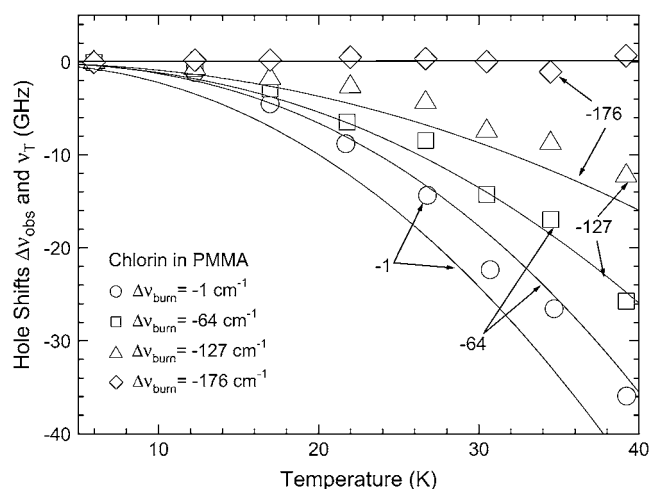

FIGURE 12 Thermal shifts of four spectral holes burned at different positions in the absorption band of chlorin in PMMA (*open symbols*). Phonon-induced shifts ν_T (*thin lines*) are calculated from Eq. 20. Hole positions are indicated with respect to 0-0 frequency in vacuum (15,912 cm^{-1} (27)).

12). As a result of thermal expansion, the negative values of $d\nu/dP$ should create a blue shift, tending to reduce thermal red shift. This component was calculated (Eq. 18) by using $d\nu/dP$ and the isochore of PMMA between 0 and 50 K ($P_V = 0.033T^{2.14}$) (see Fig. 5 in Renge (55)), and subtracted from $\Delta\nu_{obs}$, to establish the pure thermal, phonon-induced shift ν_T. The ν_T is more negative than $\Delta\nu_{obs}$, but has a weaker frequency dependence (Fig. 12). The frequency dependence of ν_T at 25 K is plotted in Fig. 11 (*solid squares*). The color effect on ν_T and QEPC constant W (Eq. 6) is in qualitative accordance with the L-J model for shifted potential minima (Eq. 17), predicting that the pressure and temperature dependencies of hole shifts should have opposite slopes (Fig. 4).

Temperature broadening of spectral holes

The thermal hole broadening can be measured in different ways (55). The broadening of a single deep and narrow hole, burned at the lowest temperature, can be recorded with the best signal/noise ratio (Fig. 10 b). This Lorentzian broadening $\Gamma(T)$ is illustrated in Fig. 11 (*open squares*) for chlorin in PMMA between 6 and 25 K. It shows little frequency dependence. However, the measurement does not provide a direct access to homogeneous line width, Γ_h, relevant to QEPC theory (Eq. 7). Besides dephasing, two additional mechanisms contribute to $\Gamma(T)$, due to spectral diffusion and the nonuniform strain fields (55).

The development of internal strains at cryogenic temperature becomes most obvious when a hole created at higher temperatures starts broadening on cooling (see Fig. 2 in Renge (55)). It has been concluded that the strain broadening is not related to baric broadening under isotropic conditions, because there is no Gaussian distortion of the hole shape (55). The strain broadening is very pronounced in polymer glasses. The polymers become very fragile when cooled to 77 K or below, and able to shatter at the slightest mechanical impact, similar to mineral glass at room temperature. The surface energy of cracks is compensated by relaxing anisotropic strains accumulated at temperatures $<T_g$. Another observation points to a build-up of internal strains on deep cooling beneath the glass point. A spontaneous disintegration of a piece of sucrose caramel takes place on dipping into liquid N_2, often accompanied with an audible click. Proteinaceous media, such as silk, wool, and leather, remain pliable when soaked in liquid nitrogen. It was confirmed that a conspicuous broadening of holes on cooling is indeed absent in the proteins as host environments (55). Plausibly, the structural hierarchy in proteins prevents the accumulation of strains at low temperatures.

A standard way of obtaining homogeneous line width Γ_h is a careful determination of quasihomogeneous width Γ_{qh} of very shallow holes created and recorded at the same temperature. As a result of self-convolution of two identical Lorentzians, Γ_{qh} would correspond to a double homogeneous

width. The broadening caused by spectral diffusion Γ_c can be derived from a thermal cycling experiment, and subtracted from Γ_{qh}, to find a theoretically relevant line width:

$$\Gamma_h = \tfrac{1}{2}(\Gamma_{qh} - \Gamma_c). \qquad (21)$$

It is clear from the given examples that narrow holes can serve as versatile probes to low-temperature properties of proteins and other biomacromolecular solids.

Comparison of the hole and the band properties

Persistent spectral hole burning in van der Waals solids is limited to $T < 50$ K, as a result of the filling and broadening of holes at higher temperature. On the other hand, spectral changes can hardly be discerned spectrophotometrically below that temperature. It is of considerable interest to link the two methods by comparing the extrapolated hole properties with the characteristics of absorption bands.

The frequency dependencies of both thermal and baric hole shifts can have important consequences with respect to broad-band behavior. A shrinking of inhomogeneous bandwidth, $\Delta\Gamma_{ih}$, due to matrix expansion can be predicted from the frequency dependence of pressure-shift coefficients $d\nu/dP$ (Fig. 11):

$$\Delta\Gamma_{ih} = -a\Gamma_{ih}P_V. \qquad (22)$$

A narrowing by 13 cm^{-1} follows from Eq. 22 in the case of chlorin-PMMA, since a is 2.25×10^{-5} bar^{-1}, inhomogeneous width Γ_{ih} at 0 K is 230 cm^{-1}, and the thermal pressure at 293 K amounts to 2600 bar (Eq. 18). This thermal dilatation effect corresponds to a reversal of pressure broadening of IDF in the L-J model (Fig. 3 b).

Another narrowing mechanism with increasing temperature derives from the frequency dependence of pure thermal, phonon-induced line shifts, ν_T, that have largest negative values on the high-frequency edge of the spectrum (Fig. 11). This mechanism is due to QEPC, and complementary to microscopic solvent shifts, affecting inhomogeneous broadening. A pronounced dependence of QEPC constant W on solvent shift is also apparent in the L-J model (Fig. 4).

The observed conspicuous color effect on thermal hole shifts (Fig. 12) results from the superposition of the above-mentioned frequency dependencies of both $d\nu/dP$ and W. A pronounced red shift at the blue edge obviously tends to squeeze the bandwidth on raising temperature. An extrapolation of the T shift curves, recorded between 6 and 40 K (Fig. 12), up to 293 K would lead to a shrinking of the chlorin absorption band, having 2hwhm of 230 cm^{-1} at 6 K, by 144 cm^{-1}, which is clearly an overestimate.

Voigtian analysis of the band shape of chlorin in PMMA reveals that the Gaussian width, Γ_G, can indeed diminish with increasing T by 12 cm^{-1} at 293 K (Table 2 and Fig. 9). A similar decrease in Γ_G was recently reported for a number of tetrapyrrolic pigments and polyarenes characterized by the S_1 spectra with weak phonon wings (DWF > 0.4) (see Table 2 in Renge (26)). The Gaussian broadening is almost absent in the S_1 and S_2 bands of Pheo a and the S_1 band of Chl a, which have a stronger, but still moderately weak, linear EPC (0.1 < DWF < 0.4) (Table 2). By contrast, Γ_G increases fast in transitions with an overwhelming phonon component, such as the Soret bands and the S_2 band of β-carotene and 1,8-DPOT. The strength of linear EPC can actually be estimated on the basis of Gaussian broadening behavior in the transitions that are nonemissive and not subject to persistent hole burning.

Gaussian hole broadening occurs at the small hydrostatic pressures below 200 bar applied in our experiments, irrespective of the direction of pressure change, with a coefficient $d\Gamma/dP$ (Fig. 10 a). The hole broadening cannot be accounted for in terms of the two-particle L-J model, and derives, perhaps, mostly from the anisotropy of intermolecular interactions. It is not clear whether the hole broadening has a counterpart in the Gaussian narrowing on dilatation of the matrix, equal to $P_V(d\Gamma/dP)$. Since in chlorin-PMMA $d\Gamma/dP$ is ~0.34 GHz/bar (Fig. 11), decrease of IDF by 30 cm^{-1} would be predicted at 293 K.

The band narrowing phenomena discussed above are superimposed with normal broadening processes due to linear and QEPC. The Lorentzian component of band broadening in chlorin from 5 to 300 K has a temperature dependence of $0.0037T^{1.71}$ (in cm^{-1} units) (Fig. 9). A much better parabolic fitting can be obtained between 5 and 200, as $0.00082T^{2.00}$. It follows from these relationships that the Lorentzian broadening would reach 1 cm^{-1} at 26 or 35 K, respectively. The quasihomogeneous hole width, equal to a double line width, is indeed ~2 cm^{-1} in this temperature range in many matrices (43). Lorentzian band broadening Γ_L was compared recently with the extrapolated homogeneous line widths Γ_h, for phthalo-naphthalocyanine in a low-density polyethylene matrix (26). Both Γ_L and the extrapolated Γ_h coincided surprisingly well and had a similar quadratic temperature dependence up to 293 K. It was assumed, tentatively, that the Lorentzian broadening reflects the dephasing rates over a broad temperature range, at least in the systems with weak linear EPC. Further investigation of the correspondence between the hole and the band broadening is needed, but it seems that a single-mode approach to dephasing rates could be reasonably valid over a very wide T range from 5 to 300 K.

Among the hole properties, the broadening components that are due to spectral diffusion and local strains have no counterpart in the band behavior. Although the spectral diffusion increases rapidly with temperature (56), it does not affect inhomogeneous bandwidth, since chromophores are moving between the potential wells on a hypersurface that remains fixed, insofar as there is no structural reorganization going on.

To summarize, the color effects on both baric and thermal shifts of holes, and perhaps the pressure broadening of holes, comprise three possible narrowing mechanisms, affecting

absorption contours on thermal expansion. QEPC contributes to the bandwidth in two opposite ways, via dynamical broadening and by means of a frequency dependence of the shift ν_T that should lead to narrowing. Linear EPC produces mainly Gaussian band broadening, and is presumed not to influence the center of gravity of the band. The narrowing phenomena reported here manifest themselves very clearly in the full width at half-maximum of the S_1 band of chlorin in PMMA, which broadens by only 1.5 cm^{-1} at 100 K and by 38 cm^{-1} at 293 K. The increase of the Lorentzian width, which can probably be identified with homogeneous broadening, is much larger, amounting to 8.5 cm^{-1} at 100 K and 73 cm^{-1} at 293 K (Fig. 9).

CONCLUSIONS

Stationary absorption spectra are complex, reflecting inhomogeneous distribution of optical transition energies, phonon side bands, and the properties of ZPLs. All contributions depend on temperature. However, due to QEPC, the shift and broadening of the lines vanish at 0 K. The absorption spectra of photosynthetic and related pigments were recorded between 6 (77) and 300 K in polymer and protein host matrices, and subject to Voigtian deconvolution. A decrease of Gaussian width in the systems with weak linear EPC was assigned to shrinking of inhomogeneous width, as a result of thermal expansion. This effect can be offset by linear EPC that causes Gaussian broadening. QEPC is responsible for Lorentzian broadening, as a consequence of exponential dephasing. It appears that QEPC does not manifest itself in multiphonon transitions, since the Lorentzian broadening is small or absent in the Soret bands of porphyrins and S_2 band of β-carotene. QEPC to matrix phonons produces a uniformly bathochromic shift.

A two-body repulsive-dispersive potential in the Lennard-Jones form was applied to predict the transformation of inhomogeneous band shapes on matrix compression. The opposite color effects on thermal and baric shifts of zero-phonon holes have been successfully accounted for. The two long-standing controversies following from potentials with coincident minima could be resolved if the upper potential well is not only deeper, but also shifted to shorter distances. Otherwise, it would be difficult to explain the absence of baric blue shifts on strong compression and thermal red shifts in the transitions with bathochromic solvent shifts.

The problem of crystalline order versus the glassy disorder in proteins has interesting implications. Bearing in mind well-defined structure of the cavities hosting pigments or other cofactors, it may seem that the inhomogeneous width should collapse on cooling to liquid He temperatures. The optical bands in proteins are narrower by a factor of 2–3 only, as compared to glassy solvents or polymers. The inhomogeneous broadening in proteins can reflect potential roughness inside the cavity and disorder in the surrounding protein and solvent glass. If the chromophore is completely embedded in the protein and not in contact with the solvent matrix, the IDF will characterize the disorder in its closest coordination layer (32).

Our model of inhomogeneous broadening incorporates the glass temperature as a key factor influencing the structural disorder in solids. As a rule, the spectral bands are sharper in frozen solvents, as compared to polymers, because the glass points of the former can be lower by several hundred K. Furthermore, the distance dependencies of intermolecular potentials are crucial parameters affecting the spectra. Electrostatic interactions that can have different signs create particularly efficient broadening mechanisms. Either the potential parameters or the compressibility of the host matrix can be estimated from the frequency-dependent pressure shifts of spectral holes. To obtain the compressibility of protein, the power coefficients and the well positions of the guest-host intermolecular potentials must be known from previous experiments or calculations.

Impurity spectroscopy has not yet exposed in full its capability of probing locally the biological environments. Ultimately, a zero-phonon transition localized on a single π-electronic chromophore can serve as a subnanoscopic sensor of the structure and dynamics of its surroundings. To achieve this, the optical probes need to be calibrated in crystalline and glassy host matrices with known properties. The limited availability of bulk material properties, including the thermal expansion coefficient, isothermal compressibility, heat conductivity and capacity, dielectric permittivity, etc., remains a serious impediment.

REFERENCES

1. Haugland, R. P. 2002. Handbook of Fluorescent Probes and Research Chemicals, 9th ed. Molecular Probes, Eugene, OR. http://probes.invitrogen.com/handbook.

2. Fritsch, C., and T. Ruzicka. 2003. Fluorescence Diagnosis and Photodynamic Therapy of Skin Diseases. Springer, New York.

3. K. Sullivan and S. Kay, editors. 1999. Green Fluorescent Proteins. Academic Press, San Diego.

4. van Amerongen, H., L. Valkunas, and R. van Grondelle. 2000. Photosynthetic Excitons. World Scientific, Singapore.

5. Mataga, N., and T. Kubota. 1970. Molecular Interactions and Electronic Spectra. Marcel Dekker, New York.

6. Reichardt, C. 2003. Solvents and Solvent Effects in Organic Chemistry. Wiley-VCH, Weinheim, Germany.

7. Rebane, K. K. 1970. Impurity Spectra of Solids. Plenum, New York.

8. Personov, R. I. 1983. Site selection spectroscopy of complex molecules in solutions and its applications. *In* Spectroscopy and Excitation Dynamics of Condensed Molecular Systems. V. M. Agranovich and R. M. Hochstrasser, editors. North-Holland, Amsterdam. 555–619.

9. Osad'ko, I. S. 1991. Optical dephasing and homogeneous optical bands in crystals and amorphous solids: dynamic and stochastic approaches. *Phys. Rep.* 206:44–97.

10. J. L. Skinner, and D. Hsu. 1986. Optical dephasing of ions and molecules in crystals. *Adv. Chem. Phys.* 65:1–44.

11. Bakshiev, N. G., O. P. Girin, and I. V. Piterskaya. 1968. Universal molecular interactions and their effect on the positions of the electronic spectra of molecules in two-component solutions. XIV. Dispersion forces and the change of molecular polarizability on optical excitation. *Opt. Spektrosk.* 24:901–909.

12. Renge, I. 1992. On the determination of molecular polarizability changes upon electronic excitation from the solvent shifts of absorption band maxima. *Chem. Phys.* 167:173–184.

13. Fitchen, D. B. 1968. Zero-phonon transitions. *In* Physics of Color Centers. W. B. Fowler, editor. Academic Press, New York. 293–350.

14. Laisaar, A. I., A. K.-I. Mugra, and M. N. Sapozhnikov. 1974. Effect of lattice vibration anharmonicity on phononless transition energies of impurity spectra of *n*-paraffin crystals. *Fiz. Tverd. Tela.* 16:1155–1158.

15. Gradl, G., J. Zollfrank, W. Breinl, and J. Friedrich. 1991. Color effects in pressure-tuned hole-burned spectra. *J. Chem. Phys.* 94:7619–7624.

16. Stübner, M., C. Hecht, and J. Friedrich. 2002. Labeling proteins via hole burning of their aromatic amino acids: pressure tuning spectroscopy of BPTI. *Biophys. J.* 83:3553–3557.

17. Lesch, H., J. Schlichter, J. Friedrich, and J. M. Vanderkooi. 2004. Molecular probes: what is the range of their interaction with the environment? *Biophys. J.* 86:467–472.

18. Renge, I. 2000. Pressure shift mechanisms of spectral holes in the optical spectra of dyes in polymer host matrices. *J. Phys. Chem. A.* 104:3869–3877.

19. Groot, M.-L., E. J. Peterman, I. H. van Stokkum, J. P. Dekker, and R. van Grondelle. 1995. Triplet and fluorescing states of the CP47 antenna complex of photosystem II studied as a function of temperature. *Biophys. J.* 68:281–290.

20. Renge, I., R. van Grondelle, and J. P. Dekker. 1996. Matrix and temperature effects on absorption spectra of β-carotene and pheophytin *a* in solution and in green plant photosystem II. *J. Photochem. Photobiol. A: Chem.* 96:109–121.

21. Francis, J. E., Jr., and S. E. Webber. 1972. Absorption spectrum of matrix-isolated Ca atoms. *J. Chem. Phys.* 56:5879–5886.

22. Shpol'skii, E. V., A. A. Il'ina, and L. A. Klimova. 1952. Fluorescence spectrum of coronene in frozen solutions. *Dokl. Akad. Nauk SSSR.* 87:935–938.

23. W. E. Moerner, editor. 1988. Persistent Spectral Hole-Burning: Science and Applications. Springer, Berlin.

24. O. Sild and K. Haller, editors. 1988. Zero Phonon Lines and Spectral Hole Burning in Spectroscopy and Photochemistry. Springer, Berlin.

25. Renge, I. 2004. Lennard-Jones model of frequency-selective baro- and thermochromism of spectral holes in glasses. *J. Phys. Chem. B.* 108:10596–10606.

26. Renge, I. 2006. Influence of temperature and pressure on shape and shift of impurity optical bands in polymer glasses. *J. Phys. Chem. A.* 110:3533–3545.

27. Even, U., and J. Jortner. 1982. Isolated ultracold porphyrins in supersonic expansions. III. Free-base porphine. *J. Chem. Phys.* 77:4391–4399.

28. Renge, I. 2000. Mechanisms of solvent shifts, pressure shifts, and inhomogeneous broadening of the optical spectra of dyes in liquids and low temperature glasses. *J. Phys. Chem. A.* 104:7452–7463.

29. Renge, I., U. Mölder, and I. Koppel. 1985. Specific and non-specific solvent effects on chlorophyll *a* visible spectral maxima. *Spectrochim. Acta A.* 41:967–971.

30. Bridgman, P. W. 1948. Rough compressions of 177 substances to 40,000 kg/cm^2. *Proc. Amer. Acad. Arts Sci.* 76:72–87.

31. Okamoto, B. Y., and H. G. Drickamer. 1974. Evaluation of configuration coordinate parameters from high pressure optical data. I. Phenanthrene, anthracene, and tetracene. *J. Chem. Phys.* 61:2870–2877.

32. Ben-Horin, N., U. Even, and J. Jortner. 1991. Microscopic and macroscopic solvation of aromatic molecules in aliphatic hydrocarbons. *Chem. Phys. Lett.* 177:153–160.

33. de Weerd, F. L., M. A. Palacios, E. G. Andrizhiyevskaya, J. P. Dekker, and R. van Grondelle. 2002. Identifying the lowest electronic states of the chlorophylls in the CP47 core antenna protein of Photosystem II. *Biochemistry.* 41:15224–15233.

34. Pullerits, T., R. Monshouwer, F. van Mourik, and R. van Grondelle. 1995. Temperature dependence of electron-vibronic spectra of photosynthetic systems. Computer simulations and comparison with experiment. *Chem. Phys.* 194:395–407.

35. Lyon, K. G., G. L. Salinger, and C. A. Swenson. 1979. Tunneling models and the experimental thermal expansivities of fused silica and poly (methylmethacrylate) (PMMA) below 4 K. *Phys. Rev. B.* 19:4231–4237.

36. White, G. K., and C. L. Choi. 1984. Thermal expansion and Grüneisen parameters of isotropic and oriented polyethylene. *J. Polym. Sci. Polym. Phys. Ed.* 22:835–846.

37. Perepechko, I. I. 1980. Low Temperature Properties of Polymers. Mir Publishers, Moscow.

38. Renge, I., and U. P. Wild. 1996. Influence of intermolecular interactions on the optical spectra of aromatic impurity molecules in solvent glasses at 8 K. *J. Lumin.* 66–67:305–309.

39. Tamm, T. B., Ya. V. Kikas, and A. E. Sirk. 1976. Measurement of the inhomogeneous distribution function of impurity centers by double scanning of the spectra. *Zh. Prikl. Spektrosk.* 24:315–321.

40. Kikas, J. V., and A. B. Treshchalov. 1983. Determination of homogeneous vibronic spectra and the inhomogeneous distribution function of impurity molecules in solids by fluorescence saturation. *Chem. Phys. Lett.* 98:295–298.

41. Tehver, I. 2004. A possibility of distinguishing the inhomogeneous broadening via coherent Raman spectra. *J. Lumin.* 107:266–270.

42. Hayes, J. M., P. A. Lyle, and G. J. Small. 1994. A theory for the temperature dependence of hole-burned spectra. *J. Phys. Chem.* 98:7337–7341.

43. Renge, I., H. Wolleb, H. Spahni, and U. P. Wild. 1997. Phthalonaphthalocyanines: new far-red dyes for spectral hole burning. *J. Phys. Chem. A.* 101:6202–6213.

44. Avarmaa, R., K. Mauring, and A. Suisalu. 1981. Reversible resonant hole burning in the fluorescence spectra of protochlorophyll. *Chem. Phys. Lett.* 77:88–92.

45. Avarmaa, R. A., and K. K. Rebane. 1985. High-resolution optical spectra of chlorophyll molecules. *Spectrochim. Acta A.* 41:1365–1380.

46. Renge, I., K. Mauring, and R. Avarmaa. 1984. High resolution optical spectra in vivo. Photoactive protochlorophyllide in etiolated leaves at 5 K. *Biochim. Biophys. Acta.* 766:501–504.

47. Renge, I., K. Mauring, and R. Vladkova. 1988. Zero-phonon transitions of chlorophyll *a* in mature plant leaves revealed by spectral hole-burning method at 5 K. *Biochim. Biophys. Acta.* 935:333–336.

48. Jankowiak, R., J. M. Hayes, and G. J. Small. 1993. Spectral hole-burning spectroscopy in amorphous molecular solids and proteins. *Chem. Rev.* 93:1471–1502.

49. Reinot, T., V. Zazubovich, J. M. Hayes, and G. J. Small. 2001. New insights on persistent nonphotochemical hole burning and its application to photosynthetic complexes. *J. Phys. Chem. B.* 105:5083–5098.

50. Hughes, J. L., B. J. Prince, E. Krausz, P. J. Smith, R. J. Pace, and H. Riesen. 2004. Highly efficient spectral hole-burning in oxygen-evolving photosystem II preparations. *J. Phys. Chem. B.* 108:10428–10439.

51. Dadarlat, V. M., and C. B. Post. 2001. Insights into protein compressibility from molecular dynamics simulations. *J. Phys. Chem. B.* 105:715–724.

52. Fidy, J., J. M. Vanderkooi, J. Zollfrank, and J. Friedrich. 1992. Softening of the packing density of horseradish peroxydase by a H-donor bound near the heme pocket. *Biophys. J.* 63:1605–1612.

53. Friedrich, J., J. Gafert, J. Zollfrank, J. Vanderkooi, and J. Fidy. 1994. *Proc. Natl. Acad. Sci. USA.* 91:1029–1033.

54. Renge, I. 2003. Thermal effects on zero-phonon holes in the optical spectra of molecular probes in polymer glasses. *Phys. Rev. B.* 68:064205.

55. Renge, I. 2002. Measurement of internal strain in polymers by means of optical hole burning. *Chem. Phys. Lett.* 357:409–414.

56. Renge, I. 1997. Spectral hole burning study of electron-phonon coupling in polymers. *J. Chem. Phys.* 106:5835–5849.